Journal of
Marine Science and Engineering

MDPI

Article

A Ship Path Tracking Control Method Using a Fuzzy Control Integrated Line-of-Sight Guidance Law

Bing Han [1,2], Zaiyu Duan [1,*], Zhouhua Peng [3] and Yuhang Chen [1,4]

1 Shanghai Ship and Shipping Research Institute Co., Ltd., Shanghai 200135, China; han.bing@coscoshipping.com (B.H.); chen.yuhang@coscoshipping.com (Y.C.)
2 College of Physics and Electronic Information Engineering, Minjiang University, Fuzhou 350108, China
3 College of Marine Electrical Engineering, Dalian Maritime University, Dalian 116026, China; zhpeng@dlmu.edu.cn
4 Merchant Marine College, Shanghai Maritime University, Shanghai 201308, China
* Correspondence: duanzaiyu1999@outlook.com

Abstract: A fuzzy control improvement method is proposed with an integral line-of-sight (ILOS) guidance principle to meet the needs of autonomous navigation and high-precision control of ship trajectories. Firstly, a three-degree-of-freedom ship motion model was established with the battery-powered container ship ZYHY LVSHUI 01 built by the COSCO Shipping Group. Secondly, a ship path-following controller based on the ILOS algorithm was designed. To satisfy the time-varying demand of the look-ahead distance parameters during the following process, especially under different navigation conditions, fuzzy logic controllers were designed for different navigation conditions to automatically adjust the look-ahead distance parameters. Thirdly, a controller was applied that uses a five-state extended Kalman filter (EKF) to estimate the heading, speed, and heading rate based on the ship's motion model with the assistance of Global Navigation Satellite System (GNSS) position measurements. This provides the necessary navigational information, reduces the algorithm's dependence on sensors, and improves its generalizability. Finally, path-following experiments were carried out in the MATLAB experimental platform, and the results were compared with different following algorithms. The simulation results showed that the new algorithm has a better following performance, and it can maintain a smooth rudder angle output. The research results provide a reference for the path-following control of ships.

Keywords: path following; ILOS guidance law; fuzzy control; extended Kalman filter

check for updates

Citation: Han, B.; Duan, Z.; Peng, Z.; Chen, Y. A Ship Path Tracking Control Method Using a Fuzzy Control Integrated Line-of-Sight Guidance Law. *J. Mar. Sci. Eng.* **2024**, *12*, 586. https://doi.org/10.3390/jmse12040586

Academic Editor: Mohamed Benbouzid

Received: 8 March 2024
Revised: 24 March 2024
Accepted: 27 March 2024
Published: 29 March 2024

1. Introduction

With the fast-paced growth of the economy and trade, there has been a surge in demand for freight transportation services. Waterborne transportation plays an indispensable role in efficiently transporting goods due to its cost-effectiveness and large capacity [1]. Container ships and other large vessels, crucial for waterway transportation, are continuously evolving towards digitization, autonomy, and intelligence to meet the ever-increasing demand for trade [2]. Autonomous ship navigation technology represents a fundamental feature of smart ships, and it also embodies the future direction of shipping technology [3]. Autonomous navigation technology needs to control the propulsion power unit according to the current position of the ship so that the ship navigates along the predetermined route, and ship path-following technology is critical to realizing this autonomous navigation of the ship, meaning it has important research significance [4].

In recent studies, there have been several approaches taken to build a simulation model for a real ship. Fossen [5] utilized a first-order model to represent the motion of the vessel. The first-order model [6] simulates the ship's course angle dynamics by mapping the rudder angle to the course angle derived from the data of the ship's maneuverability test. Song [7] employed an integral-type Abkowitz model [8] to describe the ship's motion. The

Abkowitz model approximates ship hydrodynamics by considering the vessel as an entirety and deriving third-order hydrodynamic derivatives from the Taylor expansion of motion equations. Qu [9] used a ship motion model proposed by Fossen [10], which is represented in the state space format and integrates hydrodynamic-component-based modeling with control design models based on vectors and matrices. Sandeepkumar [11] used a ship model of a KVlCC2 tanker. This modeling approach, proposed by the ship maneuvering mathematical model group (MMG) in Japan [12], is characterized by modeling the hull, propeller, and rudder separately and calculating their respective hydrodynamic forces.

In the study of path-following control, several researchers have suggested viable control strategies and addressed the related issues to different extents. Guo Jie [13] developed an Active Disturbance Rejection Controller by using the Fast Non-singular Terminal Sliding Mode. A simulation test was conducted with Dalian Maritime University's "Yulong" ship as the subject, which revealed that the controller could efficiently and accurately follow both straight and curved paths. In [14], a control law for tracking the trajectory of underactuated ships was developed by integrating the output redefinition method, an extended state observer (ESO), and the dynamic inversion control method. The design accounts for uncertainties in dynamics, external disturbances of unknown time-varying nature, and unavailable ship velocities. Ren [15] developed a time-scale decomposition method to solve the RRS control issue in path following. The resulting path-following performance is more stable and smoother. Zhu Kang [16] incorporated a deep reinforcement learning method into the LOS algorithm to suit complex control surroundings. They tested this approach using a 7 m KVLCC2 ship model, achieving a commendable tracking effect even for variable trajectories. Ghommam [17] developed a fuzzy-adaptive observer to estimate the state by solely utilizing the USVs' global position information and local measurement of the orientation angle. Le [18] integrated the Antenna Mutation Beetle Swarm Prediction Learning Algorithm into the line of sight (LOS) algorithm to address the ship parameter uncertainty issue. The algorithm's efficacy was verified through a simulation using a container ship as the test object. Renxiang Bu [19] combined a radial basis neural network with sliding mode control to accurately approximate the total unknown term and achieve precise trajectory tracking control in the presence of wind and wave currents. Huang [20] proposed an observer using internal model control (IMC), to rapidly estimate the sideslip angle in the line-of-sight guidance law, and demonstrated the efficacy of the proposed sideslip angle observer in enhancing the path-following accuracy. Xunwen Liu [21] introduced adaptive neural network and event-triggered control technology to reduce the physical damage of actuators. In recent years, linearized ship models have often been used in studies of ship path following, but actual ships have strong model and disturbance uncertainties [22], meaning that these models do not accurately reflect actual ship navigation. Meanwhile, some control algorithms are designed with idealized control inputs, which assume that theoretical values are equivalent to the real control inputs of the ship. The ship's maneuverability will be influenced by physical constraints, including limitations on the ship's rudder angle and propeller rotation speed during the voyage. Exceeding the working range limit or producing frequent jerks during maneuvering can result in significant physical damage to the ship's control mechanism. However, this approach does not align with actual engineering practice. Most researchers have focused on improving the anti-disturbance capability of an algorithm, but they have neglected the influence of the ship's maneuvering characteristics on the tracking performance under different sailing conditions. For instance, if a ship navigates along a curvilinear or twisting course, an algorithm that functions effectively on a straight trajectory will face issues such as intensified overshooting and biased oscillations, resulting in dreadful tracking performance.

In this paper, an integral line-of-sight navigation method with fuzzy control of the forward-looking distance is proposed to achieve precise path tracking in various sailing conditions. A 700 twenty-foot equivalent unit (TEU) container ship ZYHY LVSHUI 01 that operates on battery power, constructed by the COSCO Shipping Group, is chosen as the control object. Ultimately, simulation and experimental results demonstrate that the motion controller designed for the 700 TEU container ship effectively achieves path-following objectives under various conditions.

The main contributions and the key features of this paper are summarized as follows.

Using line-of-sight (LOS) navigation and fuzzy controllers, a ship motion controller is designed based on the ILOS guidance method with fuzzy control of the variable forward-looking distance. Fuzzy controllers designed for different navigational conditions can improve the performance of the algorithm by correcting the forward-looking distance parameter of the algorithm.

In this paper, a three-degree-of-freedom ship motion model is developed using the sailing data of container ship ZYHY LVSHUI 01. Furthermore, the extended Kalman filter algorithm is developed to accurately estimate speed, heading, and other states utilizing the ship's GNSS position information. This can enhance the general applicability of the control algorithm and decrease its reliance on costly sensors.

The rest of this paper is organized as follows: Section 2 introduces the ship motion model. Section 3 presents the design of the control system, including the introduction of the ILOS navigation method and its improvement. Section 4 illustrates the control algorithm's effectiveness through simulation experiments. Finally, Section 5 presents the conclusion and future work.

2. Preliminaries and Problem Statement

In this paper, a three-degree-of-freedom (DOF) mathematical model for ship maneuvering is presented, which incorporates surge, sway, and heave, based on the parameters of a 700 TEU container ship ZYHY LVSHUI 01. The 700 TEU container ship is equipped with twin engines, twin propellers, and twin rudders. See Table 1 for details of the ship parameters.

Table 1. Ship parameters.

Parameters	Values
Length	119.8 m
Draught	5.5 m
Displacement	12,600,000 kg
Rudder Area	13.02 m^2
Diameter of Propeller	2.8 m
Breadth	23.6 m
Block Coefficient	0.835
Molded Depth	9 m
Aspect Ratio of Rudder	1.355
Propulsion Power	900 kW

The equation for the ship model can be expressed as

$$\begin{cases} \begin{cases} \dot{x} = u\cos\varphi + v\sin\varphi \\ \dot{y} = u\sin\varphi + v\cos\varphi \\ \dot{\varphi} = r \end{cases} \\ (\mathrm{m} + \mathrm{m_x})\dot{u} - (\mathrm{m} + \mathrm{m_y})vr = \mathrm{X_H} + \mathrm{X_P} + \mathrm{X_R} + \mathrm{X_W} + \mathrm{X_C} \\ (\mathrm{m} + \mathrm{m_y})\dot{v} - (\mathrm{m} + \mathrm{m_x})ur = \mathrm{Y_H} + \mathrm{Y_P} + \mathrm{Y_R} + \mathrm{Y_W} + \mathrm{Y_C} \\ (\mathrm{I_{zz}} + \mathrm{J_{zz}})\dot{r} = \mathrm{N_H} + \mathrm{N_P} + \mathrm{N_R} + \mathrm{N_W} + \mathrm{N_C} \\ \mathrm{T}\dot{\delta} = \mathrm{K}\delta_c - \delta \end{cases} \tag{1}$$

where (x, y) are the position coordinates of the ship, φ is the heading angle, m is the ship's mass, $\mathrm{m_x}$, $\mathrm{m_y}$ is the added mass component along the respective direction, $\mathrm{I_{zz}}$ is the moment of inertia, $\mathrm{J_{zz}}$ represents the added moment of inertia, X, Y, and N are the external sway, surge forces, and yaw moments acting on the ship in the body reference frame, and the subscripts H, P, R, W, and C denote the forces and moments of the hull, oars, rudder, wind, and currents applied to the ship, respectively. The kinetic parameters in the equations above were calculated utilizing the empirical formulas supplied in [23]. The forces and moments on the hull are

$$\begin{cases} X_H = X(u) + X_{vv}v^2 + X_{vr}vr + X_{rr}r^2 \\ Y_H = Y_v v + Y_r r + Y_{|v|v}|v|v + Y_{|v|r}|v|r + Y_{|r|r}|r|r \\ N_H = N_v v + N_r r + N_{|v|v}|v|v + N_{vvr}v^2 r + N_{vrr}vr^2 \end{cases} \tag{2}$$

Table 2 shows the hydrodynamic coefficients calculated with empirical equations.

Table 2. Hydrodynamic coefficients.

Parameters	Values	Parameters	Values
X_{vv}	−0.0519	$Y_{\|r\|r}$	−0.0126
X_{vr}	-1.3107×10^6	N_v	−0.0737
X_{rr}	−0.065	N_r	−0.0443
Y_v	−0.3509	$N_{\|v\|v}$	−0.0112
Y_r	−0.0399	N_{vvr}	−0.2879
$Y_{\|v\|v}$	−0.1937	N_{vrr}	−0.0562
$Y_{\|v\|r}$	−0.3299		

In this paper, we maintain a constant value for the propeller speed while controlling the ship through the manipulation of the rudder. The rudder characteristics are represented using a first-order system [24]. The recommended rudder angle is indicated by δ_c, while the current rudder angle is δ. K and T represent the control gain and time constant, respectively. The maximum rudder angle is restricted to $\delta \leq \pm 35°$. The forces and moments generated by the rudder are as follows:

$$\begin{cases} X_R = (1 - t_R)F_N \sin\delta \\ Y_R = (1 + a_H)F_N \cos\delta \\ N_R = (x_R + a_H x_H)F_N \cos\delta \end{cases} \tag{3}$$

where F_N is the rudder positive pressure and the rudder parameters are as displayed in Table 3.

Table 3. Rudder parameters.

Parameters	Values
t_R	0.1844
a_H	0.8788
x_R	60
x_H	−0.4835

Then, the disturbance force on the hull is divided into two parts, wind and current, and is calculated using empirical equations. The equations below are used to calculate the disturbance forces and moments generated by the wind and the current on the hull.

$$\begin{bmatrix} X_W \\ Y_W \\ N_W \end{bmatrix} = \frac{1}{2}\rho_a V_w^2 \begin{bmatrix} C_X(\theta_w)A_{Fw} \\ C_Y(\theta_w)A_{Lw} \\ C_N(\theta_w)A_{Fw}L \end{bmatrix} \tag{4}$$

$$\begin{bmatrix} X_C \\ Y_C \\ N_C \end{bmatrix} = \frac{1}{2}\rho L d V_C^2 \begin{bmatrix} C_X(\theta_C) \\ C_Y(\theta_C) \\ C_N(\theta_C)L \end{bmatrix} \tag{5}$$

where V_w, V_c is the relative speed of wind and current, θ_w, θ_c is the relative angle of wind and current, ρ_a,ρ is the density of air and water, L is the length of the ship, d is the draft of the ship, A_{Fw} and A_{Lw} are the wind areas of the front and side of the hull, respectively, and

$C_X(\theta_w), C_Y(\theta_w), C_N(\theta_w)$ and $C_X(\theta_C), C_Y(\theta_C),\ C_N(\theta_C)$ are the wind force and current force coefficient, generally obtained from ship testing results.

The objective of this article is to design an LOS-based path-following control scheme for the target ship that enables it to travel the desired path with high accuracy, regardless of model uncertainty and unknown environmental disturbances.

3. Control System Design

The basic block diagram of the control system is shown in Figure 1. The ship features a GNSS, which obtains the ship's current location in real-time and estimates its condition through an extended Kalman filter. The ship's desired heading is calculated by ILOS with a fuzzy controller. This calculation is based on both pre-set path points and the real-time ship position. Then, the PD controller is utilized to control the rudder rotation, such that the ship can be guided to follow the pre-set path point.

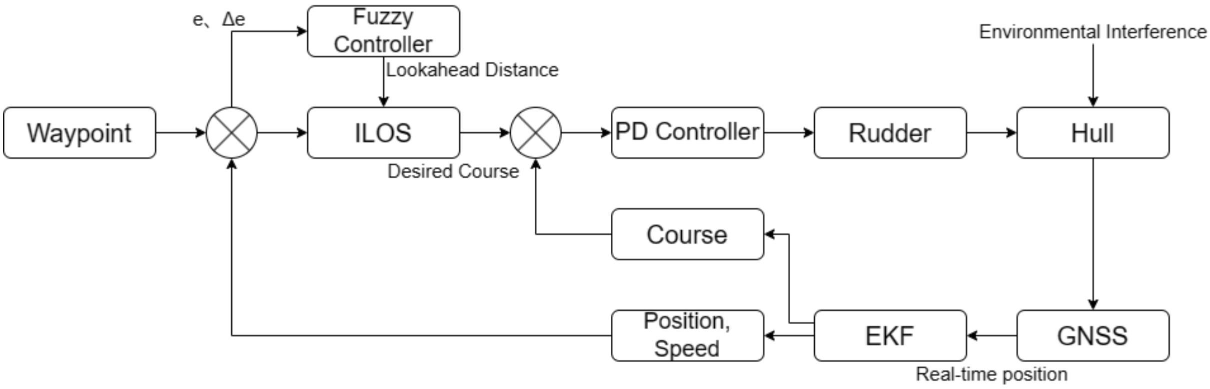

Figure 1. Basic block diagram of control system.

3.1. ILOS Guidance Method

A commonly utilized algorithm for following a path is the line-of-sight (LOS) algorithm. In Figure 2, we indicate some primary variables utilized in the ILOS algorithm.

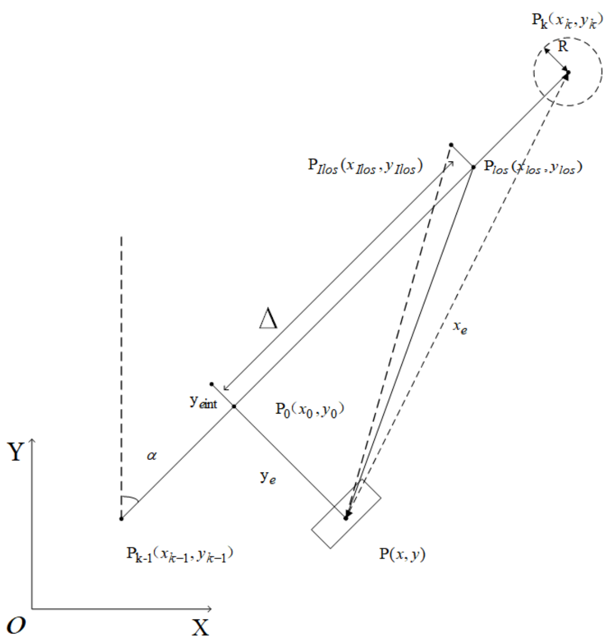

Figure 2. An illustration of the integral line-of-sight guidance.

The straight line between points $P_{k-1}(x_{k-1}, y_{k-1})$ and $P_k(x_k, y_k)$ is the line path to be followed. $P(x, y)$ represents the ship's current location while $P_0(x_0, y_0)$ is the point where the ship's location intersects the path. Then, the direction angle of the path can be calculated using

$$\alpha = \text{atan2}\left(\frac{y_k - y_{k-1}}{x_k - x_{k-1}}\right) \tag{6}$$

Following this, we could compute the along-track and cross-track errors (y_e, x_e) by using

$$\begin{cases} y_e = -(x - x_k)\sin\alpha + (y - y_k)\cos\alpha \\ x_e = (x - x_k)\cos\alpha + (y - y_k)\sin\alpha \end{cases} \tag{7}$$

When the along-track distance x_e is less than R, the LOS algorithm goes to the next waypoint. In the traditional LOS algorithm [10], the desired heading χ is calculated based on

$$\chi = \alpha - \text{atan2}\left(\frac{y_e}{\Delta}\right) \tag{8}$$

where Δ is the looking-ahead distance. However, conventional LOS guidance is not equipped to manage an environmental disturbance, such as wind or current. Accordingly, Borhaug [25] proposed the ILOS algorithm:

$$\begin{array}{c} \chi = \alpha - \text{atan2}\left(\frac{y_e + \kappa y_{eint}}{\Delta}\right) \\ \dot{y}_{eint} = \frac{\Delta y_e}{\Delta^2 + (y_e + \kappa y_{int})^2} \end{array} \tag{9}$$

where $\kappa > 0$ is a designed integral gain. In [26], a different version of the integral LOS algorithm is proposed as follows:

$$\begin{array}{c} \chi = \alpha - \text{atan2}\left(\frac{y_e + \kappa y_{eint}}{\Delta}\right) \\ \dot{y}_{eint} = \frac{U y_e}{\sqrt{\Delta^2 + (y_e + \kappa y_{int})^2}} \end{array} \tag{10}$$

where U is the absolute speed. From Figure 2 with Equations (9) and (10), the integral term indicates that the desired heading angle will be a non-zero constant when $y_e = 0$. This enables the use of a portion of the ship's forward speed to counteract the effects of the flow disturbance. Algorithm 1 provides the pseudo-code for the LOS/ILOS algorithm.

Algorithm 1: LOS/ILOS

Inputs: ship location (x, y); waypoint (wp.x,wp.y)
Output: desired heading angle χ

1. k $\leftarrow$ 1 (initialization); set R; set LOS/ILOS parameter Δ, κ
2. Initialization starting point (xk, yk) $\leftarrow$ (wp.x(k), wp.y(k)), and end point (xk_next, yk_next) $\leftarrow$ (wp.x(k + 1), wp.y(k + 1))
3. Compute the path angle α
4. Compute the along-track and cross-track errors (x_e, y_e)
5. If x_e < R_switch, then k=k+1, end
6. Compute the desired heading angle χ

If the ship's position is far from the intended path, the accumulation of error can easily lead to integration saturation and result in overshoot. Therefore, this study employs a combination of the ILOS and LOS navigation methods [27], as illustrated in Figure 3. If $y_e < \mathrm{L_{pp}}$, the controller employs the ILOS navigation method, and if $y_e \geq \mathrm{L_{pp}}$, the controller shall utilize the LOS navigation method.

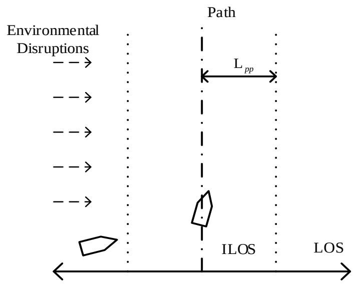

Figure 3. Area schematic.

3.2. Fuzzy-Rule-Based Lookahead Distance Selection Method

The performance of the ILOS algorithm can be enhanced by modifying the parameter for lookahead distance. A shorter lookahead distance typically leads to more aggressive steering and faster attainment of the desired path, but it may also cause unwanted oscillations around it. Conversely, a longer lookahead distance results in smoother steering that prevents such oscillations but has the disadvantage of slower convergence to the path. The fuzzy controller is designed to dynamically adjust the forward-looking distance of the ILOS navigation method by using fuzzy rules based on the deviation e and the difference in the deviation Δe. The process of formulating the mapping from a given input to an output using fuzzy logic is known as the fuzzy inference system (FIS). The fuzzy inference system type utilized in this paper is the "Sugeno Fuzzy Inference System" [28]. The first step is to define the inputs and outputs of the system and determine the degree to which they belong to each corresponding fuzzy set using Gaussian membership functions. In this paper, the inputs to the system include the deviation $e = [-50, 50]$ and the difference in the deviation $de = [-0.3, 0.3]$, while the output is the look-ahead distance $\Delta = [100, 300]$. Then, in the second step, the center-of-area approach, also known as the center-of-gravity method, is the most widely used defuzzification procedure in fuzzy logic control. Essentially, it is

$$u = \frac{\sum_{i=1}^{N} w_i z_i}{\sum_{i=1}^{N} w_i} \tag{11}$$

where N is the number of quantization levels of the output, z_i is the value of the output at quantization level, and w_i represents its membership value in the output fuzzy set. The final step is to define fuzzy rules for different navigational conditions.

Overall, when the ship moves away, we decrease the forward-looking distance to accelerate steering. Conversely, when the ship moves closer, we increase the forward-looking distance to minimize overshooting. In the line condition, the target ship follows a predetermined path on a straight course from a distant position, and the fuzzy controller determines the motion trend of the ship using the deviation e and the difference in the deviation de. If both the deviation e and the difference in the deviation de are positive, it indicates that the ship is moving away from the reference path. In this case, even if e is small, the look-ahead distance Δ needs to be reduced. Conversely, if the deviation e and the difference in the deviation de are in opposite directions, it means that the ship is close to the reference path. Therefore, the value of L needs to be increased appropriately to prevent overshooting. The resulting fuzzy rule table for the line condition is shown in Table 4.

Table 5 shows the design of fuzzy rules for curvilinear conditions, which follows the same logic as that of line conditions. In curvilinear conditions, a ship will make multiple turns. The curvature of the route and the disturbance of the flow will cause a larger deviation. To decrease steering bias, the ship's lookahead distance should be reduced even more, prompting the ship to steer more assertively and ultimately reducing steering bias.

Table 4. Components of fuzzy rules for the line condition.

de	*e*						
	NB	**NM**	**NS**	**ZO**	**PS**	**PM**	**PB**
NB	PVS	PS	PS	PM	PB	PM	PVS
NS	PVS	PS	PM	PB	PM	PS	PVS
ZO	PVS	PM	PS	PB	PM	PS	PVS
PS	PVS	PS	PM	PB	PM	PS	PVS
PB	PVS	PM	PB	PM	PS	PVS	PVS

Table 5. Components of fuzzy rules for the curvilinear condition.

de	*e*						
	NB	**NM**	**NS**	**ZO**	**PS**	**PM**	**PB**
NB	PVS	PVS	PVS	PS	PVS	PVS	PVS
NS	PVS	PS	PM	PM	PM	PS	PVS
ZO	PVS	PM	PS	PB	PM	PS	PVS
PS	PVS	PS	PM	PM	PM	PS	PVS
PB	PVS	PVS	PVS	PS	PVS	PVS	PVS

In a turning condition, the ship's heading angle is constantly adjusted, resulting in changing environmental disturbances and deviations that make it difficult for the error to converge to zero. To counter the effects of environmental disturbances, the change in the difference in the deviation *de* determines the magnitude of the disturbances and adjusts the lookahead distance dynamically. The ultimate components of the fuzzy rules are shown in Table 6.

Table 6. Components of fuzzy rules for the turning condition.

de	*e*						
	NB	**NM**	**NS**	**ZO**	**PS**	**PM**	**PB**
NB	PVS	PVS	PS	PS	PB	PM	PVS
NS	PVS	PS	PM	PM	PM	PS	PVS
ZO	PVS	PS	PS	PB	PS	PS	PVS
PS	PVS	PS	PM	PM	PM	PS	PVS
PB	PVS	PM	PB	PS	PS	PVS	PVS

3.3. Extended Kalman Filter

Researchers sometimes assume that the ship navigation subsystem is available as the perception system, and that the ship control system can access the necessary information directly. To obtain precise navigational information, such as speed and course, ships require costly sensory equipment. So, to improve the generalizability of control algorithms and eliminate the need for sensing equipment, it is necessary to accurately estimate the information required for control. To achieve a precise estimation of variables such as speed and direction and enhance the robustness of the algorithm, in this study, a five-state extended Kalman filter algorithm [29] is employed to estimate the ship's speed, course angle, and other variables utilizing positional data from the GNSS. The dynamics of a ship following a path can be modeled by using a combination of the CV and CA models [30,31] according to

$$\begin{cases} \dot{x}^n = U\cos(\chi) \\ \dot{y}^n = U\sin(\chi) \\ \dot{U} = -\alpha_1 U + \omega_1 \\ \dot{\chi} = \omega_\chi \\ \dot{\omega}_\chi = -\alpha_2 \omega_\chi + \omega_2 \end{cases} \tag{12}$$

where (x^n, y^n) is the north-east position of a ship, ω_1 and ω_2 are Gaussian white-noise processes, and two constants (α_1, α_2) from the Singer model [32] have been incorporated into the model so that U and ω_χ converge to zero during stationkeeping [33]. The discrete form of the equation is

$$\begin{cases} x^n[k+1] = x^n[k] + \mathrm{h}U[k]\sin(\chi[k]) \\ y^n[k+1] = y^n[k] + \mathrm{h}U[k]\sin(\chi[k]) \\ U[k+1] = (1-\mathrm{h}\alpha_1)U[k] + \mathrm{h}\omega_1[k] \\ \chi[k+1] = \chi[k] + \mathrm{h}\omega_1[k] \\ \omega_\chi[k+1] = (1-\mathrm{h}\alpha_2)\omega_\chi[k] + \mathrm{h}\omega_2[k] \end{cases} \tag{13}$$

where h is the sampling time. Then, the GNSS measurement equations are

$$\begin{cases} y_1 = x^n + \varepsilon_1 \\ y_2 = y^n + \varepsilon_2 \end{cases} \tag{14}$$

where ε_1 and ε_2 are Gaussian white-noise measurement noise. The discrete-time forms are

$$\begin{cases} y_1[k] = x^n[k] + \varepsilon_1[k] \\ y_2[k] = y^n[k] + \varepsilon_2[k] \end{cases} \tag{15}$$

The discrete-time state–space model becomes

$$\begin{aligned} \boldsymbol{x}[k+1] &= \boldsymbol{A}_d\boldsymbol{x}[k] + \boldsymbol{E}_d\boldsymbol{\omega}[k] \\ \boldsymbol{y}[k] &= \boldsymbol{C}_d x[k] + \boldsymbol{\varepsilon}[k] \end{aligned} \tag{16}$$

where $\boldsymbol{x} = [x^n, y^n, U, \chi,\ \omega_\chi]^T, \boldsymbol{y} = [x^n, y^n]^T, \boldsymbol{\omega} = [\omega_1,\ \omega_2]^T$, and

$$\begin{gathered} \boldsymbol{A_d} = \begin{bmatrix} 1 & 0 & \cos(\hat{\chi})\mathrm{h} & -\mathrm{h}\widehat{U}[k]\sin(\hat{\chi}) & 0 \\ 0 & 1 & \sin(\hat{\chi})\mathrm{h} & \mathrm{h}\widehat{U}[k]\cos(\hat{\chi}) & 0 \\ 0 & 0 & 1-\mathrm{h}\alpha_1 & 0 & 0 \\ 0 & 0 & 0 & 1 & \mathrm{h} \\ 0 & 0 & 0 & 0 & 1-\mathrm{h}\alpha_2 \end{bmatrix} \\ \boldsymbol{E_d} = \begin{bmatrix} 0 & 0 \\ 0 & 0 \\ \mathrm{h} & 0 \\ 0 & 0 \\ 0 & \mathrm{h} \end{bmatrix}, \quad \boldsymbol{C}_d = \begin{bmatrix} 1 & 0 & 0 & 0 & 0 \\ 0 & 1 & 0 & 0 & 0 \end{bmatrix} \end{gathered} \tag{17}$$

Extended Kalman filter algorithms based on motion models then become [33]
Initial values:

$$\begin{gathered} \hat{\boldsymbol{x}}^-[0] = \boldsymbol{x}_0 \\ \widehat{\boldsymbol{P}}^-[0] = E\Big[\big(\boldsymbol{x}[0] - \hat{\boldsymbol{x}}^-[0]\big)\big(\boldsymbol{x}[0] - \hat{\boldsymbol{x}}^-[0]\big)^T\Big] = \boldsymbol{P}_0 \end{gathered} \tag{18}$$

Kalman filter gain:

$$\boldsymbol{K}[k] = \widehat{\boldsymbol{P}}^-[k]\boldsymbol{C}_d^T[k]\Big(\boldsymbol{C}_d[k]\widehat{\boldsymbol{P}}^-[k]\boldsymbol{C}_d^T[k] + \boldsymbol{R}_d[k]\Big)^{-1} \tag{19}$$

Corrector:

$$\begin{gathered} \hat{\boldsymbol{x}}[k] = \hat{\boldsymbol{x}}^-[k] + \boldsymbol{K}[k]\big(\boldsymbol{y}[k] - \mathrm{h}\big(\hat{\boldsymbol{x}}^-[k]\big)\big) \\ \widehat{\boldsymbol{P}}[k] = (\boldsymbol{I} - \boldsymbol{K}[k]\boldsymbol{C_d}[k])\widehat{\boldsymbol{P}}^-[k](\boldsymbol{I} - \boldsymbol{K}[k]\boldsymbol{C_d}[k])^{\boldsymbol{T}} + \boldsymbol{K}[k]\boldsymbol{R_d}[k]\boldsymbol{K^T}[k] \end{gathered} \tag{20}$$

Predictor:

$$\begin{gathered} \hat{\boldsymbol{x}}^-[k+1] = \boldsymbol{A_d}\hat{\boldsymbol{x}}[k] + \boldsymbol{B_d}\boldsymbol{u}[k] \\ \widehat{\boldsymbol{P}}^-[\boldsymbol{k}+1] = \boldsymbol{A_d}\widehat{\boldsymbol{P}}[k]\boldsymbol{A}_d^T + \boldsymbol{E_d}\boldsymbol{Q_d}[k]\boldsymbol{E}_d^T \end{gathered} \tag{21}$$

where $h\left(\hat{x}^{-}[k]\right) = C_d[k]\hat{x}^{-}[k]$, and where $Q_d[k]$and $R_d[k]$ are the process covariance and measurement matrices, respectively.

4. Simulations

In this section, the 700ETU motion model is used as the test object to verify the effectiveness of the modified ILOS algorithm. The motion mathematical model's dynamic parameters are extensively outlined in Section 2. The ship motion model and Kalman filter estimation algorithm were tested using the Zig-Zag and turning tests. Simulation tests were also performed using the traditional LOS algorithm, Borhaug's ILOS algorithm, Lekkas' ILOS algorithm, and the modified ILOS algorithm, respectively, to demonstrate the advantages of the modified ILOS algorithm. The test algorithms utilized the PD controller for heading control, while the other three control algorithms used a fixed lookahead distance parameter, which was set to twice the length of the ship.

4.1. Test Simulation Model

In this section of our work, the Zig-Zag test and turning test were conducted to verify the maneuverability and applicability of the 700 TEU container ship simulation model. In addition, the extended Kalman filter from Section 3 was used for parameter estimation during the test.

First, the 20°/20° Zig-Zag test procedure involves the following steps: (1) Initially, the container ship is sailing at a speed of 12 n mile/h (about 6 m/s). After approaching steadily, it rapidly steers 20° to starboard and maintains the rudder angle. (2) When the ship's heading is 20° off the initial course, the rudder is rapidly turned to the port side at 20° and maintained. (3) Finally, this process is repeated until the end of the test. In Figure 4, the test results show that the first overshoot angle is about 4.5° which is in accordance with the maneuvering standards. This also confirms that the EKF can estimate the speed and course angle with great precision during the Zig-Zag test.

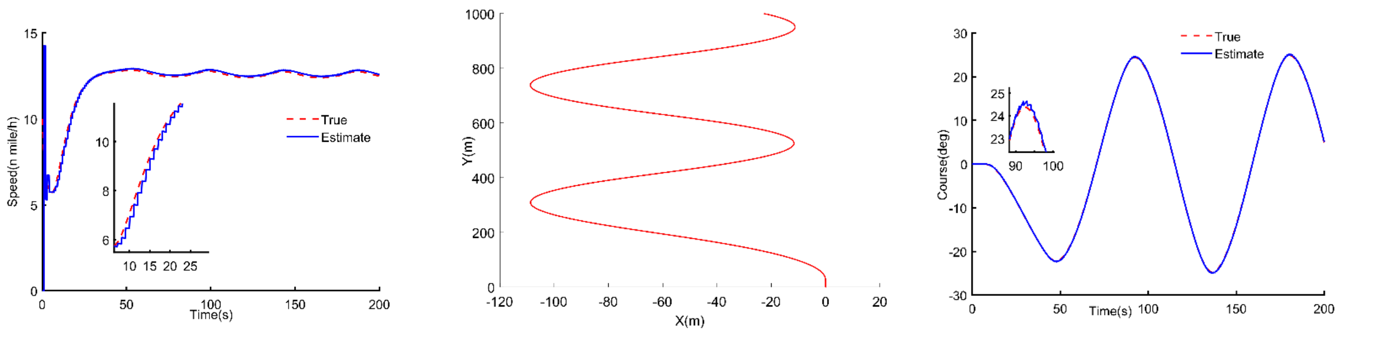

(**a**) (**b**) (**c**)

Figure 4. The Zig-Zag simulation test: (**a**) speed estimate; (**b**) ship's trajectory; (**c**) course estimate.

For the turning test, the process begins with the ship maintaining a constant speed of 12 n mile/h (about 6 m/s). Next, the rudder is turned to the maximum right angle of 35° and remains in this position until the ship completes a full turning circle beyond 360°.

Figure 5 shows that in the turning test, the ship's advance distance (Ad) at 90° is approximately 323 m, and the tactical diameter distance (DT) at 180° is 616 m. It is important to note that the Ad of the turning circle is less than three times the Lpp (length of perpendicular) of the ship, which is about 120 m; and the DT of the turning circle is about six times the Lpp. During the turning test, the EKF obtains accurate estimates of the speed and the course angle.

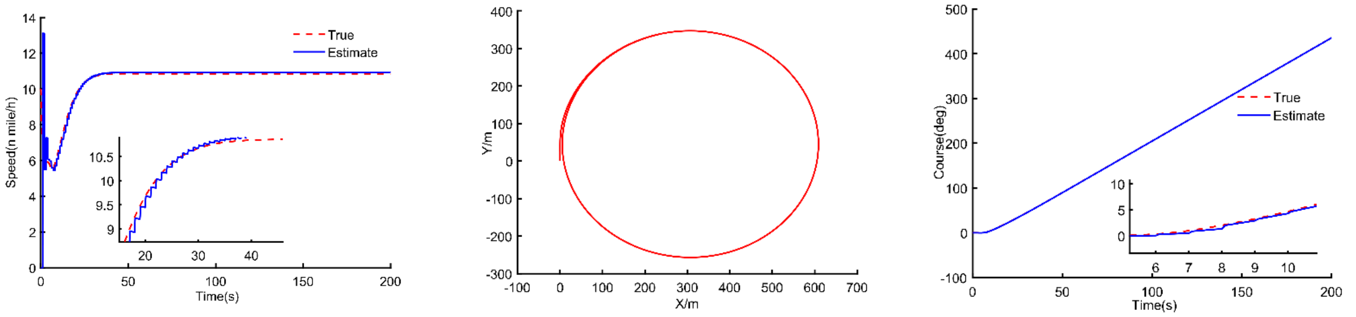

(**a**) (**b**) (**c**)

Figure 5. The turning simulation test: (**a**) speed estimate; (**b**) ship's trajectory; (**c**) course estimate.

From the results of the tests above, it can be concluded that the vessel has good maneuverability, while the performance of the EKF is generally acceptable for engineering application.

4.2. Line Path-following Test

In the line path-following test, the desired path begins at the coordinates (1500, 0) and concludes at (1500, 9000). The ship's initial position is (0, 0) and it is heading east. The ship's speed is set at 10 n mile/h, while the wind speed is 1.5 m/s with a wind angle of 45°, and the current speed is 2.2 m/s with a current angle of 45°. The simulation results using the modified ILOS algorithm are illustrated by the red line in Figure 6. Figure 6a,b show that the ship under the modified ILOS algorithm can follow the reference path with satisfactory control performance. The algorithm's final following error is 1 m, with only 5 m of overshoot during the following process. In Figure 6c,d, the controlled ship displays a more reasonable and smooth change in rudder angle and speed. Moreover, the simulation results under the other three algorithms are also shown in Figure 6. Figure 6b illustrates that the traditional LOS algorithm is susceptible to environmental disturbances, resulting in a fixed error of approximately 15 m that cannot be eliminated. Meanwhile, the rest of the ILOS algorithms offset the influence of the environmental interference, and the final convergence error reaches within 1 m. However, the two ILOS algorithms produce overshoots of 117 m and 22 m under the influence of the fixed lookahead parameters and the integral term, respectively. Then, Figure 6c,d show that the control inputs of the other algorithms for the rudder angle have reached the maximum limit of the rudder, resulting in a significant reduction in speed. Consequently, the simulation comparison results indicate that the proposed algorithm can achieve a satisfactory following performance. Moreover, it maintains a reasonable rudder angle and speed. Table 7 compares the performance metrics of different algorithms, including the overshooting, the final following error, and the time required for the error to converge. The modified algorithm has improved convergence speed, reduced tracking error, and significantly decreased overshooting during the convergence process.

Table 7. Comparison of line path-following performance.

	Overshooting/m	Errors/m	Time/s
LOS	none	15	300
Borhaug's ILOS	117	1	190
Lekkas's ILOS	22	1	200
Modified ILOS	5	1	200

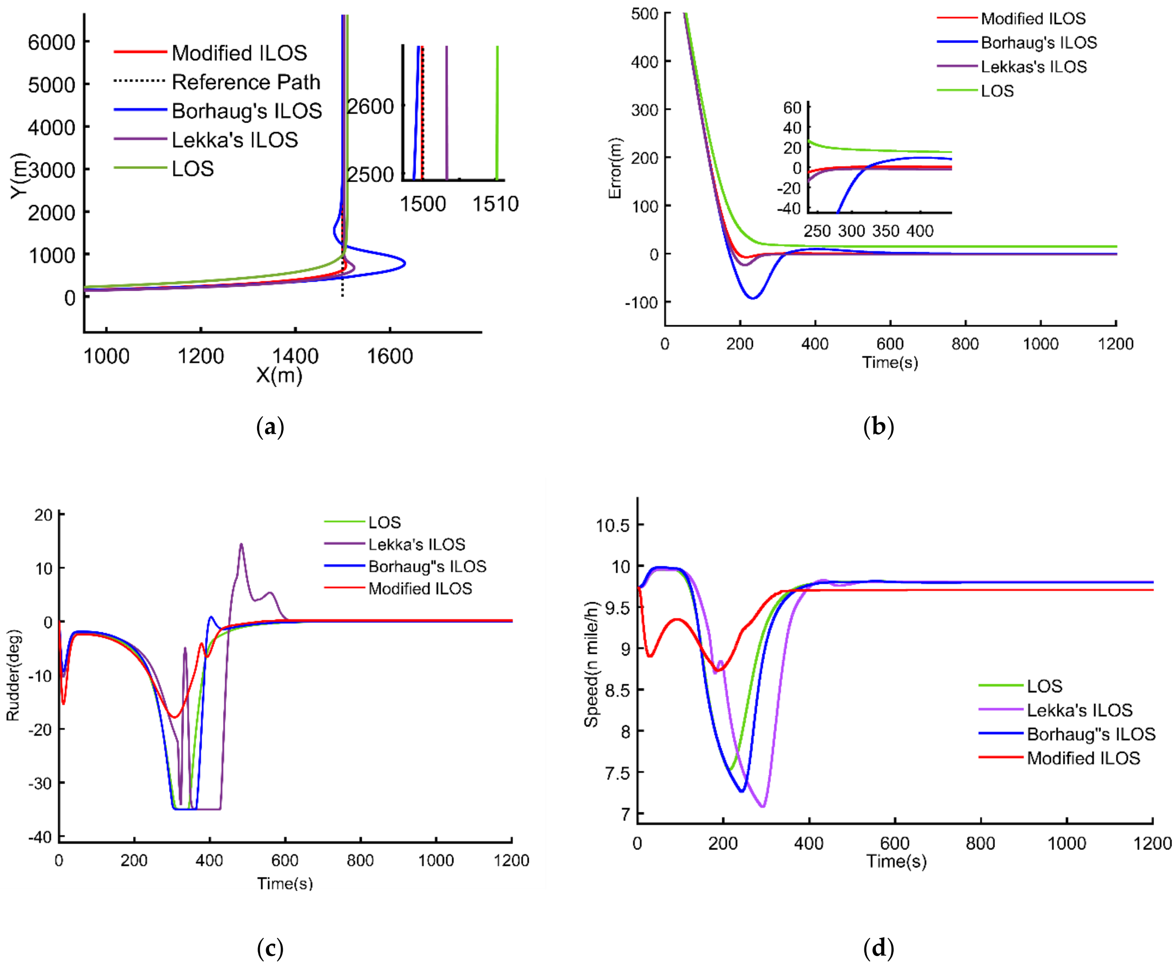

Figure 6. Line path-following simulation results: (**a**) path-following performance; (**b**) cross-tracking errors; (**c**) rudder angles; (**d**) speeds.

4.3. Curvilinear Path-Following Test

In the curvilinear path-following test, the reference path is

$$\begin{cases} X = 500a \\ Y = 500\cos(a) \end{cases} \tag{22}$$

where $a = [0, 4\pi]$, the ship's initial position is $(-100, 500)$, and it is heading east. The ship's speed is set at 10 n mile/h, while the wind speed is 1.5 m/s with a wind angle of 45°, and the current speed is 2.2 m/s with a current angle of 45°. The simulation results using the modified ILOS algorithm are illustrated by the red line in Figure 7. Figure 7a shows the performances of the four algorithms, which are all capable of following the reference path. Based on Figure 7b it can be observed that the proposed algorithm has the smoothest convergence process, completing convergence in 220 s with a following error of 1 m. Figure 7c,d exemplify the changes in the rudder angle and ship speed during the following process. The proposed algorithm can maintain stability during the ship's multiple course adjustments by adjusting the lookahead distance through the fuzzy rule.

In Figure 7c, the regulation of the rudder angle displays minimal fluctuations, indicating a consistent and stable control. In Figure 7d, the ship's speed shows a steady cyclic variation. Table 8 presents a comparison of the performance indices of the algorithms. It can be observed that the proposed algorithm has the smoothest convergence process, completing convergence in 220 s with a following error of 1 m. The proposed modified ILOS algorithm can maintain stability during the ship's multiple course adjustments by adjusting the lookahead distance through the fuzzy rule. This contrasts with the other algorithms, which produce large jitter due to heading changes.

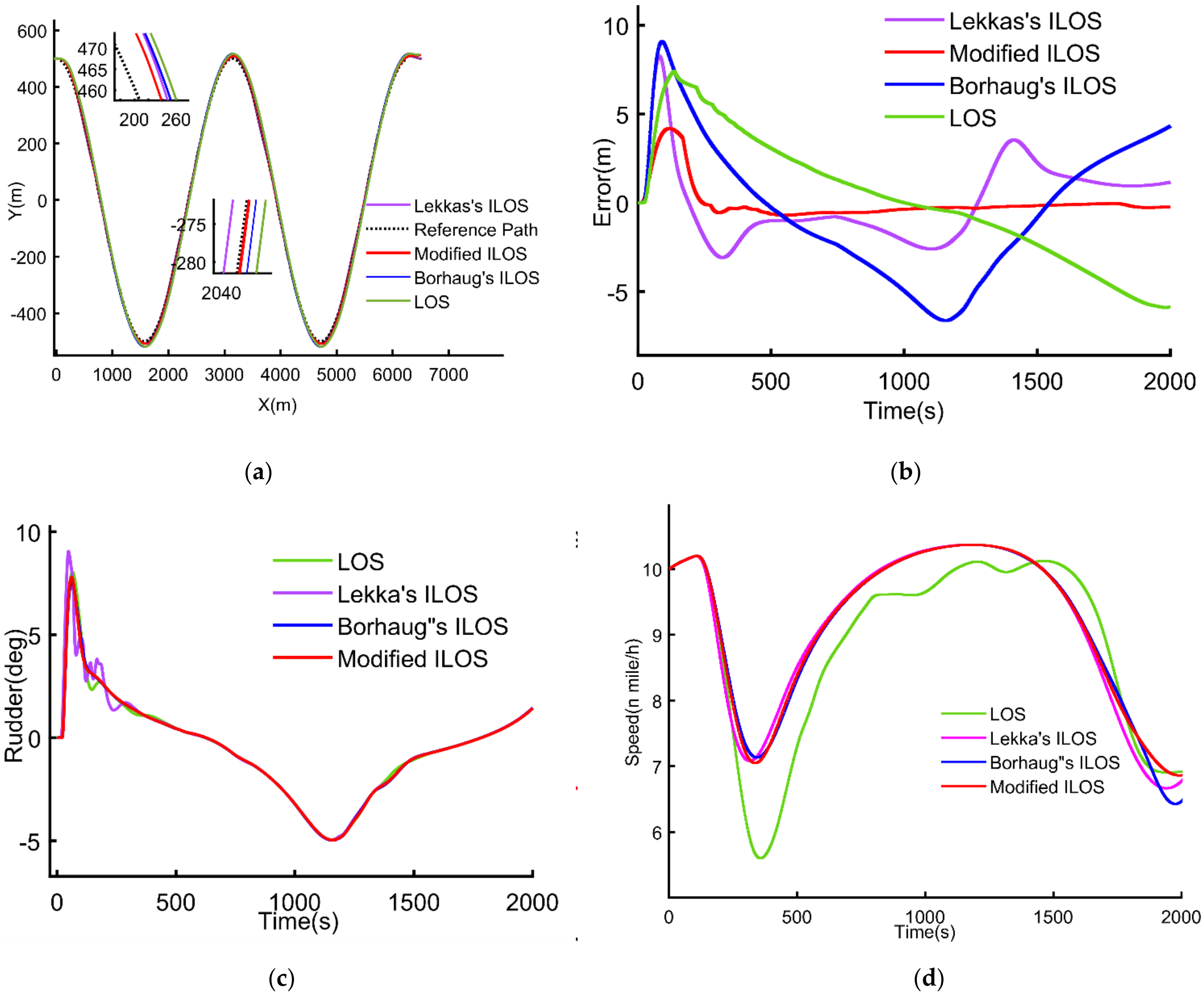

Figure 7. Curvilinear path-following simulation results: (**a**) path-following performance; (**b**) cross-tracking errors; (**c**) rudder angles; (**d**) speeds.

Table 8. Comparison of Curvilinear path-following performance.

	Overshooting/m	Errors/m	Time/s
LOS	7.5	8	1160
Borhaug's ILOS	9.6	8	580
Lekkas's ILOS	8.3	4	190
Modified ILOS	4.2	1	220

4.4. Turning Path-Following Test

In the turning path-following test, the reference path is

$$\begin{cases} X = 1500\sin(a) \\ Y = 1500\ \cos(a) \end{cases} \tag{23}$$

where $a = [0,\ 4\pi]$, the ship's initial position is $(-100,\ 1500)$, and it is heading east. The ship's speed is set at 10 n mile/h, while the wind speed was 1.5 m/s with a wind angle of 45°, and the current speed is 2.2 m/s with a current angle of 45°. The simulation results are shown in Figure 8 and the performance quantification indices are summarized in Table 9. Figure 8a shows that the proposed algorithm can drive the ship along the desired path with a high-precision process. Figure 8b shows that the proposed algorithm can converge the error quickly, whereas the other algorithm has an obvious oscillation during the process. Under turning conditions, the ship is subject to continuously changing environmental disturbances and the influence of path curvature. This makes a portion of the following error difficult to converge. The LOS algorithm conventionally has a constant following error of 7 m when following the reference slewing trajectory and is unable to converge. While Borhaug's ILOS algorithm can slowly reduce the following error to 3 m in 2000 s under the effect of the integral term, Lekkas's ILOS algorithm has a much faster error convergence and converges the following error to 1 m in 1500 s. The algorithm mentioned above cannot be adjusted according to the actual navigation situation as it uses a fixed lookahead distance parameter. Therefore, there is still room for improvement in its performance. The fuzzy rule enables the algorithm to use lower lookahead parameters during turning conditions compared to straight line conditions. This prompts the ship to perform more aggressive steering to eliminate errors. The following error is reduced to 1 m at 500 s without generating unstable oscillations. In Figure 8c,d, the controlled ship displays a more reasonable and smooth change in rudder angle and speed. Hence, in this case, the modified ILOS algorithm path-following control method is more effective and robust according to these simulation results.

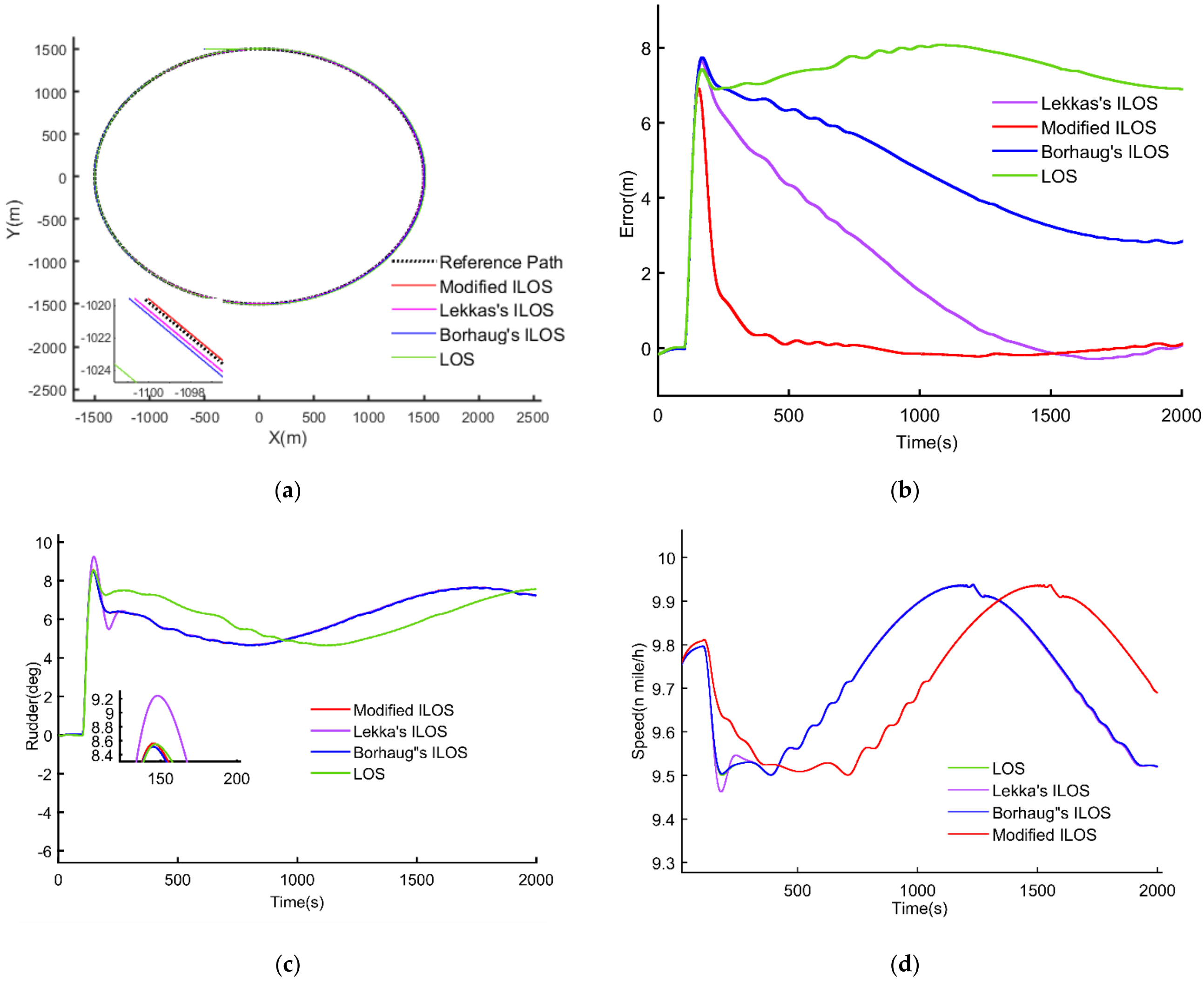

Figure 8. Turning path-following simulation results: (**a**) path-following performance; (**b**) cross-tracking errors; (**c**) rudder angles; (**d**) speeds.

Table 9. Comparison of Turning path-following performance.

	Overshooting/m	Errors/m	Time/s
LOS	7.9	7	2000
Borhaug's ILOS	7.9	3	2000
Lekkas's ILOS	7.8	1	1500
Modified ILOS	7.5	1	500

5. Conclusions

In this paper, a fuzzy-controlled-variable forward-looking-distance ILOS guidance law has been presented to meet the needs of autonomous ship navigation and high-precision ship trajectory control. Fuzzy rules designed for various navigation conditions can improve the accuracy and convergence speed by adjusting the algorithm's lookahead distance parameter. In addition, the algorithm does not rely on accurate ship models or sensing devices, but rather utilizes the EKF algorithm to estimate the ship's state via GNSS position data, making the algorithm both generalizable and universal. Simulation and experimental results have demonstrated that that a ship under the modified ILOS algorithm has satisfactory following results for line, curvilinear, and turning paths, and it performs more reasonable maneuvers compared to when using other algorithms. Meanwhile, it was concluded from Tables 7–9 that the proposed control algorithm can converge the tracking error to within 1 m under the three working conditions with high tracking accuracy, and it also has a faster and better convergence process compared to other comparative algorithms. The results attest to its comprehensive advantages, which are of great significance for achieving autonomous navigation and high-precision control of ship trajectories.

In future research, obstacles and automatic collision avoidance should be considered in path following. Furthermore, since the ship motion model is calculated by using mainly empirical formulas, it can be further optimized to improve the accuracy of the ship motion model.

Author Contributions: B.H.: Conceptualization, Methodology, Supervision, Visualization, Funding Acquisition, Writing—Review and Editing; Z.D.: Conceptualization, Data Curation, Writing—Original Draft, Software, Validation, Writing—Review and Editing; Z.P.: Investigation, Conceptualization, Project Administration, Supervision, Validation, Writing—Review and Editing; Y.C.: Conceptualization, Data Curation, Formal Analysis, Funding Acquisition, Investigation, Project Administration, Writing—Review and Editing. All authors have read and agreed to the published version of the manuscript.

Funding: This research was funded by the National Key R&D Program of China, grant number 2022YFC2807004; the Natural Science Foundation of the Fujian Province of China, grant number 2022J011128; and the Shanghai Science Program for a Shanghai Academic/Technology Research Leader, grant number 23XD1431000.

Institutional Review Board Statement: Not applicable.

Informed Consent Statement: Not applicable.

Data Availability Statement: Data are contained within the article.

Acknowledgments: The authors would like to thank the editor and two reviewers for their useful feedback that improved this paper.

Conflicts of Interest: The authors declare no conflicts of interest.

References

1. Yan, X.P. Implementing self-reliance and scientific and technological innovation to open new horizons for high-quality development of Yangtze River shipping. *China Water Trans.* **2021**, *11*, 12–15.
2. Li, Y.Z.; Zheng, Z.; Wu, T.; Dou, Z.X. Introduction to Development Trend and Challenges of Smart Ships in Era of Industry 4.0. *Ship Eng.* **2023**, *45*, 224–229.
3. Li, Y.J.; Zhang, R.; Wei, M.H.; Zhang, Y. State-of-the-art research and prospects of key technologies for ship autonomous navigation. *Chin. J. Ship Res.* **2021**, *16*, 32–44.

4. Yu, Y.L.; Su, R.B.; Fong, X. Tracking control of backstepping adaptive path of unmanned surface vessels based on surge-varying LOS. *Chin. J. Ship Res.* **2019**, *14*, 163–171.
5. Fossen, T.I. Line-of-sight path-following control utilizing an extended Kalman filter for estimation of speed and course over ground from GNSS positions. *J. Mar. Sci. Technol.* **2022**, *27*, 806–813. [CrossRef]
6. Nomoto, K.; Taguchi, T.; Honda, T.; Hirano, S. On the Steering Qualities of Ships. *J. Zosen Kiokai* **1956**, *99*, 75–82. [CrossRef]
7. Song, L.; Xu, C.; Hao, L.; Yao, J.; Guo, R. Research on PID Parameter Tuning and Optimization Based on SAC-Auto for USV Path Following. *J. Mar. Sci. Eng.* **2022**, *10*, 1847. [CrossRef]
8. Abkowitzm, A. Measurement of hydrodynamic characteristic from ship maneuvering trials by system identification. *Trans. Soc. Nav. Archit. Mar. Eng.* **1980**, *88*, 283–318.
9. Qu, X.; Jiang, Y.; Zhang, R.; Long, F. A Deep Reinforcement Learning-Based Path-Following Control Scheme for an Uncertain Under-Actuated Autonomous Marine Vehicle. *J. Mar. Sci. Eng.* **2023**, *11*, 1762. [CrossRef]
10. Fossen, T.I. *Handbook of Marine Craft Hydrodynamics and Motion Control*; John Wiley & Sons: Hoboken, NJ, USA, 2021.
11. Sandeepkumar, R.; Rajendran, S.; Ranjith, M.; Antonio, P. A unified ship manoeuvring model with a nonlinear model predictive controller for path following in regular waves. *Ocean. Eng.* **2021**, *243*, 110165. [CrossRef]
12. Ogawa, A.; Kasai, H. On the mathematical model of manoeuvring motion of ship. *Int. Ship-Build. Prog.* **1978**, *25*, 306–319. [CrossRef]
13. Guo, J.; Liu, Y.H.; Ma, L.H. Active Disturbance Rejection Control for Ship Trajectory Tracking with Multimodal Fast Nonsingular Terminal Sliding Mode Strategy. *Navig. China* **2020**, *43*, 7–13.
14. Tan, C.; Du, J.L.; Xu, G.X.; Li, D.H. Trajectory Tracking Control Design of Underactuated Ships Based on ESO and Dynamic Inversion. *Ship Eng.* **2020**, *42*, 103–109.
15. Ren, R.-Y.; Zou, Z.-J.; Wang, J.-Q. Time-Scale Decomposition Techniques Used in the Ship Path-Following Problem with Rudder Roll Stabilization Control. *J. Mar. Sci. Eng.* **2021**, *9*, 1024. [CrossRef]
16. Zhu, K.; Huang, Z.; Wang, X.M. Tracking control of intelligent ship based on deep reinforcement learning. *Chin. J. Ship Res.* **2021**, *16*, 105–113.
17. Jawhar, G.; Maarouf, S.; Faisal, M. Prescribed performances based fuzzy-adaptive output feedback containment control for multiple underactuated surface vessels. *Ocean. Eng.* **2022**, *249*, 110898.
18. Le, W.; Li, S.J.; Liu, J.L.; Qing, W. Data-driven path-following control of underactuated ships based on antenna mutation beetle swarm predictive reinforcement learning. *Appl. Ocean. Res.* **2022**, *124*, 103207.
19. Zhang, H.G.; Bu, R.X.; Yu, J.M. RBF neural network sliding mode control for ship path following. *J. Shanghai Marit. Univ.* **2021**, *42*, 7–11.
20. Huang, Y.; Shi, X.; Huang, W.; Chen, S. Internal Model Control-Based Observer for the Sideslip Angle of an Unmanned Surface Vehicle. *J. Mar. Sci. Eng.* **2022**, *10*, 470. [CrossRef]
21. Liu, X.W.; Xu, C.; Chen, Z.F. Event-triggered adaptive PID trajectory tracking control for marine surface vechles. *J. Shanghai Marit. Univ.* **2023**, *44*, 11–17.
22. Li, W.; Xie, H.W.; Han, J.Q.; Meng, F.B. Track control of Under-actuated ship based on Model Free Adaptive PD Control. *Ship Sci. Technol.* **2022**, *44*, 21–25.
23. Jia, X.L.; Yang, Y.S. *Mathematical Model of Ship Motion*; Dalian Maritime University Press: Dalian, China, 1998.
24. Liu, C.; Li, T.S.; Chen, N.X. Dynamic surface control and minimal learning parameter (DSC-MLP) design of a ship's autopilot with rudder dynamics. *J. Harbin Eng. Univ.* **2012**, *33*, 9–14.
25. Borhaug, E.; Pavlov, A.; Pettersen, K.Y. Integral LOS control for path following of underactuated marine surface vessels in the presence of constant ocean currents. In Proceedings of the 2008 47th IEEE Conference on Decision and Control, Cancun, Mexico, 9 December 2008.
26. Lekkas, A.M. *Guidance and Path-Planning Systems for Autonomous Veicles*; Norwegian University of Science and Technology: Trondheim, Norway, 2014.
27. Huang, C.P.; Zou, Z.J.; He, H.W.; Fan, J. Path following and collision avoidance of underactuated ships based on model predictive control and modified particle swarm optimization. *Navig. China* **2023**, *46*, 125–134.
28. Sugeno, M. *Industrial Applications of Fuzzy Control*; Elsevier: Amsterdam, The Netherlands, 1985.
29. Brown, R.A.; Phil, H. *Introduction to Random Signals and Applied Kalman Filtering*; John Wiley & Sons: Hoboken, NJ, USA, 2012.
30. Li, X.R.; Jilkov, V. Survey of Maneuvering Target Tracking. Part I. Dynamic Models. *IEEE Trans. Aerosp. Electron. Syst.* **2003**, *39*, 1333–1364.
31. Siegert, G.; Bany's, P.; Martinez, C.S.; Heymann, F. EKF Based Trajectory Tracking and Integrity Monitoring of AIS Data. In Proceedings of the 2016 IEEE/ION Position, Location and Navigation Symposium (PLANS), Savannah, GA, USA, 11–14 April 2016.
32. Singer, R.A. Estimating Optimal Tracking Filter Performance for Manned Maneuvering Targets. *IEEE Trans. Aerospace Electron. Syst.* **1970**, *AES-6*, 473–483.
33. Fossen, S.; Fossen, T.I. Five-State Extended Kalman Filter for Estimation of Speed over Ground (SOG), Course over Ground (COG) and Course Rate of Unmanned Surface Vehicles (USVs): Experimental Results. *Sensors* **2021**, *21*, 7910. [CrossRef]